THE JOURNAL OF PHYSICAL CHEMISTRY C

Article

pubs.acs.org/JPCC

In Situ Dissolution–Diffusion toward Homogeneous Multiphase Ag/Ag_2S@ZnS Core–Shell Heterostructures for Enhanced Photocatalytic Performance

Ting Zhu,[†] Chun Zhang,[‡,§] and Ghim Wei Ho*[,†,∥]

[†]Department of Electrical and Computer Engineering, National University of Singapore, 4 Engineering Drive 3, 117576, Singapore

[‡]Department of Physics, National University of Singapore, 2 Science Drive 3, 117542, Singapore

[§]Department of Chemistry, National University of Singapore, 3 Science Drive 3, 117543, Singapore

[∥]Engineering Science Programme, National University of Singapore, 4 Engineering Drive 3, 117576, Singapore

ABSTRACT: Multiphase Ag/Ag_2S@ZnS of homogeneous hybrid core–shell heterostructures with distinctive hierarchical structures have been prepared. The manipulation of composition and structure by virtue of localized Ag ions dissolution–diffusion within the ZnS shell structure is demonstrated to facilitate homogeneous hybridization between Ag/Ag_2S and ZnS. In addition to the presence of Ag/Ag_2S core, the in situ hybridization optimizes contact interface for heterojunction-induced charge transfer, an outstanding challenge commonly faced in photocatalyst design. This work also validates integration of multicomponent material to form a complex hybrid heterostructure that is not accessible by conventional synthesis methodology. Finally, this work concludes with proof of concept demonstrating the feasibility of employing the as-prepared multiphase Ag/Ag_2S@ZnS core–shell heterostructures as visible to UV light responsive photocatalyst for solar H_2 production.

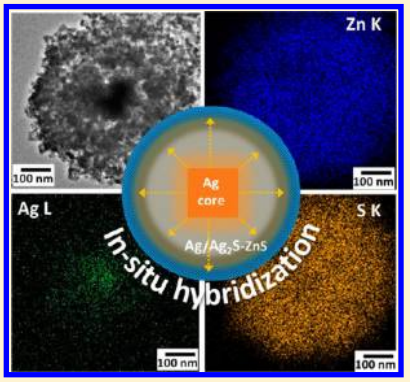

1. INTRODUCTION

Development of a synthetic approach to prepare strategically not only porous core–shell nanocomposite but one that consists of two or more material components presents a promising way to achieve unique physicochemical properties.[1−5] Porous core–shell nanostructures have attracted considerable interest in the area of catalysis owing to their attributes of high surface area, structural stability, and optimal contact interface for enhancing electronic and catalytic exploitations.[6−8] Meanwhile, heterostructures of two or more distinct materials such as semiconductor and noble metal (e.g., Pd/TiO_2, Cu_2O/TiO_2, Au@TiO_2, Ag@SnO_2, etc.) have also received much attention due to their credit of altering the electronic structure of the host material to achieve higher activity and/or stability than their pure phase/composition equivalent.[9−15]

Synthesis of core–shell heterostructures of diverse material components is usually based on a template-engaged approach, in which the cores are coated with different shell materials followed by the subsequent selective removal of cores by dissolution or calcination.[16−22] However, it is a strategically challenging process because of the disparate growth processes involving incompatible growth kinetics, mechanisms, and reaction rates.[8] Though there are some recent reports on the fabrication of multiphase heterostructures with diverse properties and functionalities, these methods are usually cost, time, and labor demanding.[23−32] Furthermore, the functionalities of these hybrid nanostructures are not well-explored alongside with the ability to manipulate their structures and compositions toward development of new functional materials with novel physical and chemical properties. Hence, integrating different structural and chemical composition to form complex and homogeneous hybrid nanostructures through facile approaches remains a challenging task yet an exciting field to be explored.

In this work, to the best of our knowledge, we have for the first time prepared multiphase Ag/Ag_2S@ZnS core–shell heterostructures with tailored chemical compositions through a hydrothermal chemical transformation. Herein, Ag nanocubes are first employed as cores for initial mesoporous silica (m-SiO_2) coating to form Ag@m-SiO_2 before the growth of zinc silicate (Zn-silicate). Then, the subsequent Ag@m-SiO_2@Zn-silicate is hydrothermally transformed into Ag/Ag_2S@ZnS core–shell structures by sulfurization in the presence of thiourea. Notably, the one-step sulfurization process serves not only to remove the silica coating but also to allow convenient conversion of Ag to Ag/Ag_2S hybrid core and Zn silicate to ZnS shell. More importantly, with the control of sulfurization, a homogeneous dissolution and diffusion of Ag ions throughout the core–shell structure can be realized. Uniquely, this in situ chemical transformation from the core to the shell structure aims to facilitate intimate and homogeneous hybridization of multiphase materials which can desirably mitigate the limited interfacial contact and charge transfer challenges faced in a typical photocatalyst design. As a proof of

Received: October 16, 2014
Revised: January 5, 2015
Published: January 9, 2015

DOI: 10.1021/jp510413b
J. Phys. Chem. C 2015, 119, 1667−1675

concept, various hybrid heterostructures are compared as UV to visible light activated photocatalysts for H_2 production. Evidently, the employed hydrothermal chemical transformation is a powerful approach toward hierarchical structural design and interfacial engineering of multiphase nanomaterials that can also be generically extended to other metal/metal oxide−semiconductor systems for various applications.

2. EXPERIMENTAL SECTION

Synthesis of Ag Nanocubes and Ag@m-SiO_2. The preparations of Ag nanocubes and Ag@m-SiO_2 nanocolloids were based on a previous work with slight modifications.[33] Briefly, 200 mL of ethylene glycol (EG) was added into a 250 mL blue-cap glass bottle and heated in an oil bath to 150 °C under vigorous magnetic stirring. Then the bottle was kept at 150 °C for another 60 min under uncapped conditions, followed by the addition of 2.5 mL of NaHS (3 mM in EG) and 30 mL of polyvinylpyrrolidone (PVP, Mw = 55 000, 20 mg mL^{-1} in EG). After the temperature was increased to 150 °C, 10 mL of $AgNO_3$ (48 mg mL^{-1} in EG) was added dropwise into the bottle, and the mixture was stirred for another 70 min before it was cooled to room temperature (RT) in an ice bath. The Ag nanocubes were washed and collected by rinse−centrifugation process with acetone and DI water for several times. The as-prepared Ag nanocubes were redispersed into 10 mL of ethanol for further use. For the m-SiO_2 coating, 1 mL of the above suspension was dispersed into 10 mL of DI water and 90 mL of ethanol by ultrasonication for 30 min followed by the addition of 0.18 g of hexadecyltrimethylammonium bromide (CTAB) and 2 mL of ammonia (28 wt %). After 5 min, 0.3 mL of tetraethyl orthosilicate (TEOS) was added into the mixture under vigorous magnetic stirring, and the reaction was continued to be stirred at RT for 4 h. The light gray products were washed with ethanol and DI water for several times by rinse−centrifugation and then dried at 60 °C in an air-flow oven for 24 h.

Synthesis of Ag@m-SiO_2@Zn-Silicate. A 20 mg portion of the as-prepared Ag@m-SiO_2 was dispersed into 40 mL of DI-water by ultrasonication for 15 min, followed by the addition of 1.2 g of urea for the activation of the SiO_2 surface. After sonication for another 10 min, 0.5 mL of $Zn(NO_3)_2$ (0.1M) was added into the solution. The mixture was sealed in a glass bottle and then heated at 102 °C in an oven for 12 h. The reaction is allowed to cool down naturally, and the products were collected by the rinse-centrifugation process with DI water and ethanol several times. The obtained products are thoroughly dried at 60 °C in an air-flow oven for 24 h for the next-step usage.

Synthesis of Ag/Ag_2S@ZnS. In order to prepare Ag/Ag_2S@ZnS heterostructures, 30 mg of the as-prepared Ag@m-SiO_2@Zn-silicate was first dispersed into 30 mL of solution containing 15 mL of DI water and 15 mL of ethanol by sonication for 15 min. Later, 100/200 mg of thiourea was added into the solution, and the mixture was transferred into Teflon and sealed in an autoclave before heated at 125 °C for 12 h. After the reaction, the autoclave was allowed to cool down naturally, and the gray products were collected by the rinse−centrifugation with DI-water and ethanol several times. Before being sent for various characterizations, the obtained products were dried thoroughly at 60 °C in a vacuum oven for 12 h. As a comparison, pure ZnS nanoparticles assembled from nanosheets were also prepared using m-SiO_2 nanocolloids (no Ag cores inside) as hard template at a thiourea dosage of 200 mg. For the purpose of clear demonstration, Ag/Ag_2S@ZnS heterostructures sulfurized through 100, 200, and 300 mg of thiourea, and pure ZnS without cores are marked as sample Ag/Ag_2S@ZnS-I, Ag/Ag_2S@ZnS-II, Ag/Ag_2S@ZnS-III, and ZnS, respectively, throughout the text.

Materials Characterizations. All the samples are characterized by field-emission scanning electron microscopy (FESEM, JEOL FEG JSM-7001F) equipped with an energy dispersive X-ray spectroscopy (EDX), transmission electron microscopy (TEM, Philips FEG CM300) equipped with elemental mapping system, and X-ray diffraction (XRD, Philips X-ray diffractometer, Cu Ka). X-ray photoelectron spectroscopy (XPS), VGSCALAB 220I-XL, system equipped with an Mg Kα X-ray source was employed to study the elemental compositions. The N_2 adsorption and desorption isotherms were measured at 77 K by a Quantachrome NOVA-1200 system. The BET surface area was calculated using adsorption data in a relative pressure ranging from 0.05 to 0.3. Absorption spectra of the samples are measured with a UV−vis−NIR spectrophotometer (UV−vis, Shimadzu UV-3600).

H_2 Evolution Measurements. The photocatalytic reactions are conducted in a quartz cylindrical glass tube of 25 mL in volume. A 10 mg portion of the as-prepared photocatalysts are weighted into the glass tube and dispersed into 10 mL of Na_2S/Na_2SO_3 aqueous solution ($[Na_2S]$ = 0.35 M, $[Na_2SO_3]$ = 0.25 M) by sonication for 5 min. The glass tube is sealed and purged with argon gas (Ar) for 10 min before the mixture is stirred vigorously in a metal box. A 300 W xenon arc lamp equipped with a cutoff filter (λ > 400 nm) is used to provide incident visible light. Gas samples are analyzed using a gas chromatograph (Shimadzu GC2014) to determine the amount of H_2.

3. RESULTS AND DISCUSSION

The synthetic strategy for preparation of Ag/Ag_2S@ZnS and pure ZnS nanostructures is schematically shown in Figure 1.

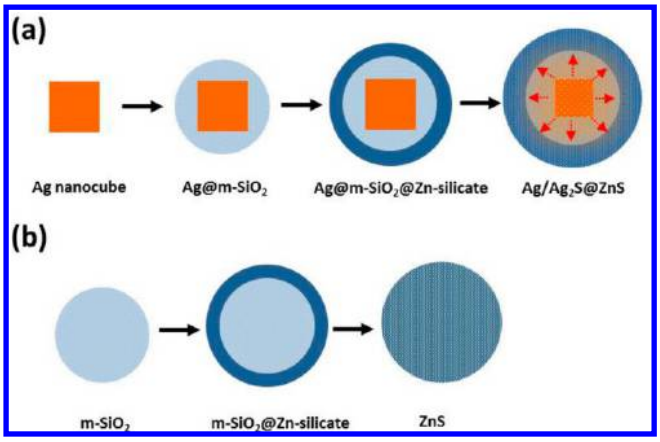

Figure 1. Schemes of the synthesis for Ag/Ag_2S@ZnS (a) and ZnS (b).

Figure 1a shows the Ag-engaged synthesis for Ag/Ag_2S@ZnS heterostructures. Herein Ag nanocubes are used as a hard template as well as a silver source for silica coating to form Ag@m-SiO_2 core−shell structures. Next, hierarchically structured Zn-silicates are grown onto the Ag@m-SiO_2 surface, which results in the formation of Ag@m-SiO_2@Zn-silicate. Finally, the Ag@m-SiO_2@Zn-silicate is converted into Ag/Ag_2S@ZnS by a hydrothermal chemical transformation with the assistance of

DOI: 10.1021/jp510413b
J. Phys. Chem. C 2015, 119, 1667−1675

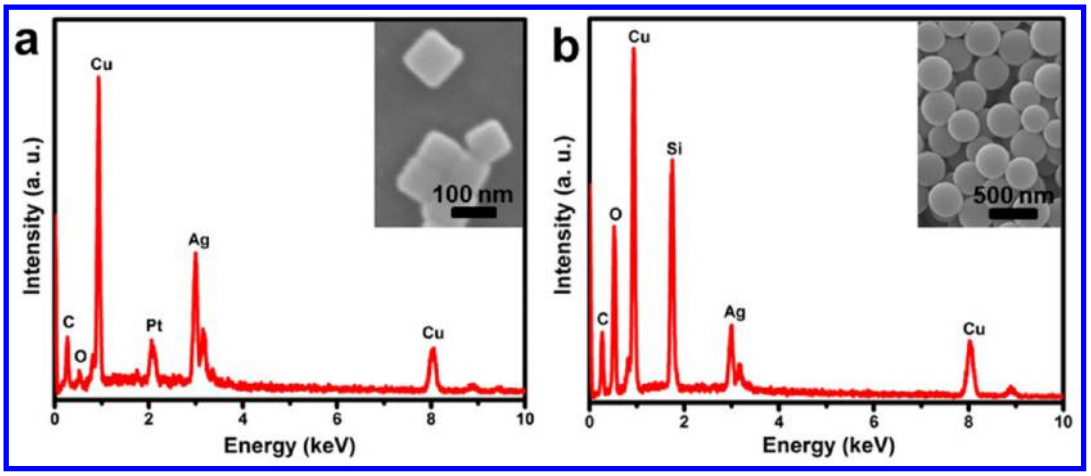

Figure 2. EDX and FESEM (insets) of Ag nanocubes (a) and Ag@m-SiO_2 (b).

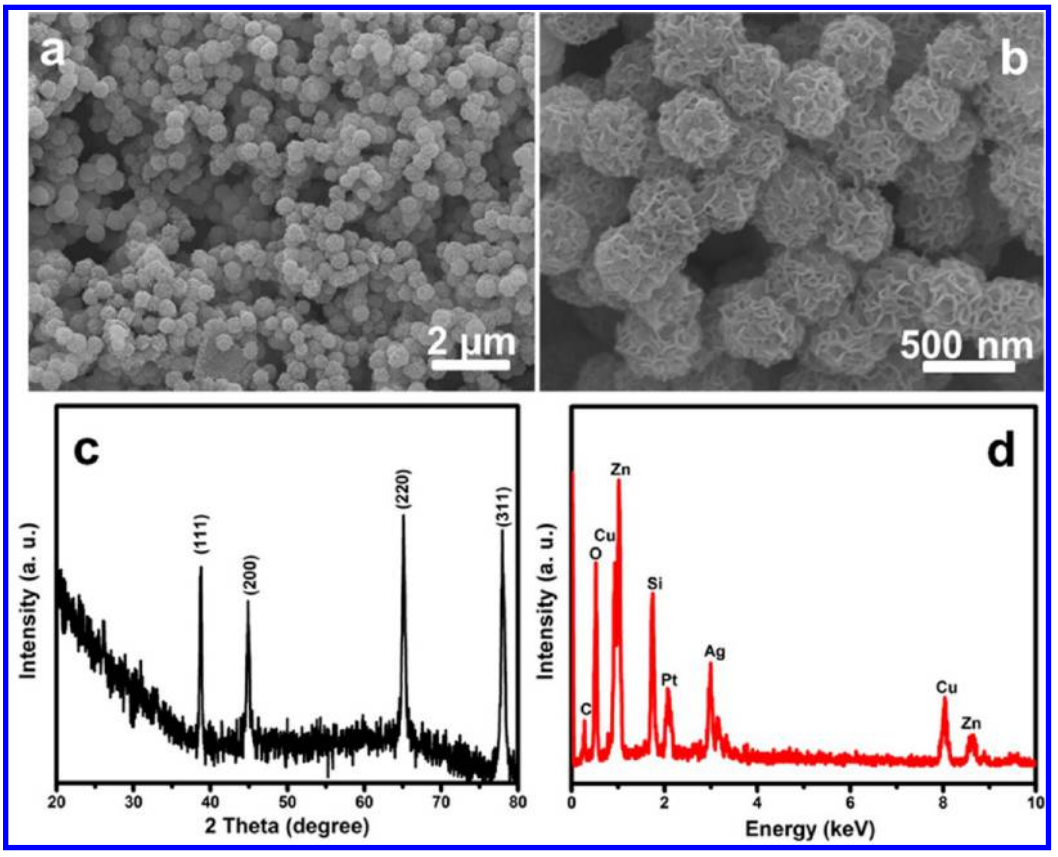

Figure 3. FESEM images (a and b), XRD pattern (c), and EDX (d) of the as-prepared Ag@m-SiO_2@Zn-silicate.

thiourea. With the control of sulfurization, homogeneous dissolution and diffusion of Ag ions throughout the core−shell structure forms multiphase hybrid between Ag/Ag_2S and ZnS shells. In addition, similar synthetic procedure is carried out to prepare ZnS nanosheets with empty core using 200 mg of thiourea without employing Ag nanocubes as cores as depicted in Figure 1b.

The FESEM and EDX results of the Ag nanocubes (~100 nm in size) and Ag@m-SiO_2 (380 nm on average) are presented in Figure 2. The EDX was performed on Cu substrates throughout this work. The appearance of strong peaks of Si and O as well as Ag after silica coating confirms the chemical composition of Ag@m-SiO_2. After deposition of Zn-silicate, the uniform morphology of as-grown nanostructures is shown in Figure 3a. The magnified FESEM image (Figure 3b) shows that the Zn-silicate formed on Ag@m-SiO_2 shows nanosheet morphology with an average particle size of 540 nm. This indicates that an average shell thickness of Zn-silicate is ~80 nm. All the indexed peaks of XRD pattern shown in Figure 3c can be attributed to cubic phase of metallic Ag (JCPDS 65-2871).[34] The undetected silica and Zn-silicate XRD peaks may be due to their amorphous structure.[33] However, the presence of Zn-silicate can be detected by EDX, where sharp peaks of Zn, Si, and O can be clearly observed (Figure 3d).

After sulfurization by the hydrothermal chemical transformation method, the as-formed Ag@m-SiO_2@Zn-silicate

DOI: 10.1021/jp510413b
J. Phys. Chem. C 2015, 119, 1667−1675

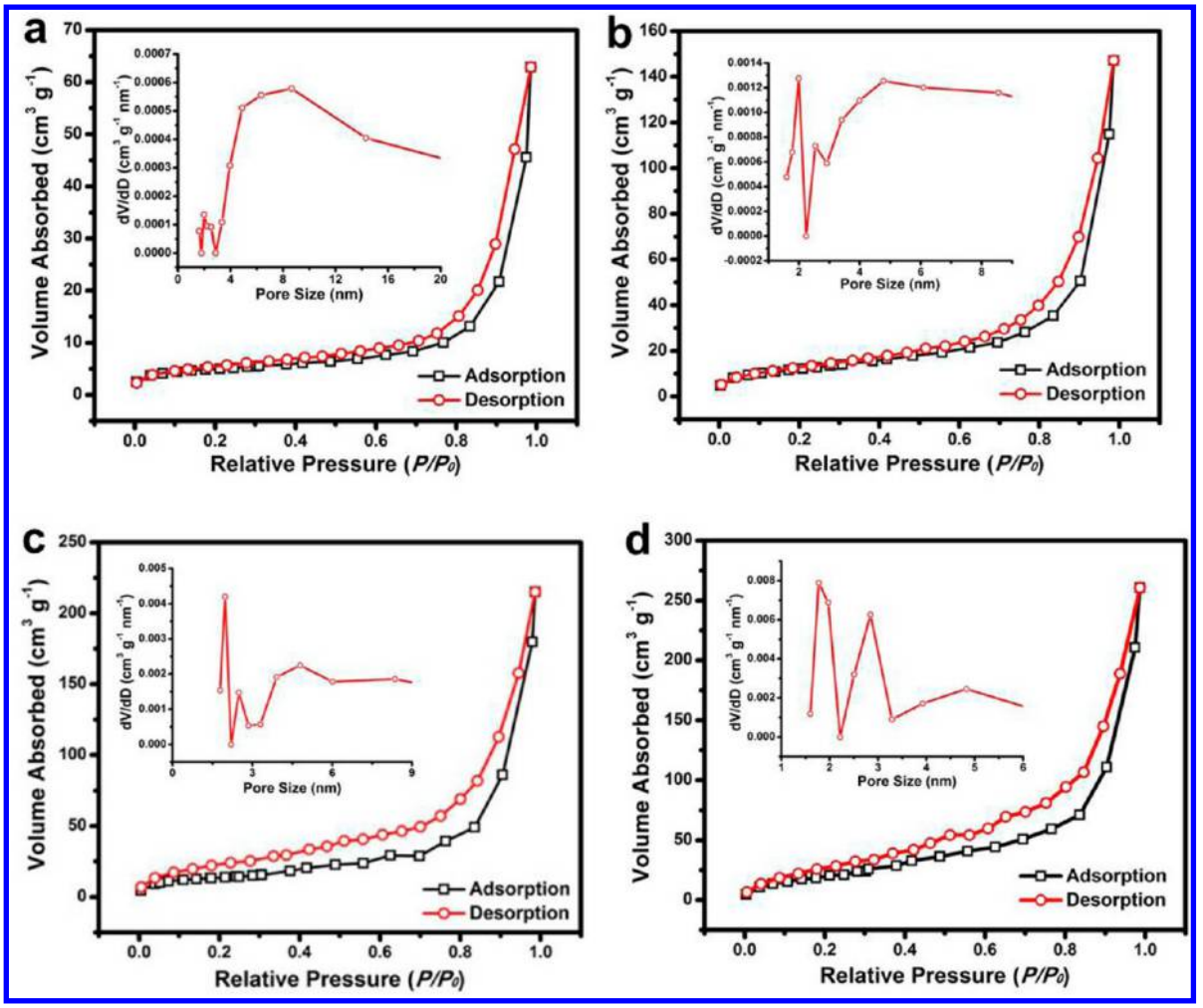

Figure 4. BET results of the samples Ag/Ag_2S@ZnS-I (a), Ag/Ag_2S@ZnS-II (b), Ag/Ag_2S@ZnS-III (c), and ZnS (d). The insets show the corresponding pore size distributions obtained from desorption isotherms.

nanostructures are converted into multiphase heterostructures with porous texture. The BET results show that specific surface areas of 17, 44, 84, and 79 $m^2\ g^{-1}$ with pore size distributions of 6, 2−6, 1.5−3, and 2−3 nm are obtained for Ag/Ag_2S@ZnS-I, Ag/Ag_2S@ZnS-II, Ag/Ag_2S@ZnS-III, and ZnS, respectively (Figure 4). It is speculated that the Ag dissolves during the sulfurization process. The hydrolysis of thiourea in hydrothermal system has resulted in the release of OH^- and S^{2-}, leading to a highly alkaline and sulfur-rich atmosphere. The precoated silica layer is then etched which may facilitate the out-diffusion of Ag ions from the core areas to the shell structure. At the same time, the S^{2-} diffuses into the interior of the particles to react with the Ag^+ to form Ag_2S, achieving the homogeneous distribution of Ag_2S. Evidently, the Ag/Ag_2S@ZnS-I sample shows uniform sheet-like hierarchical structures (Figure 5a). Furthermore, TEM image in Figure 5b clearly shows well-preserved nanosheet shell structures and nanocube cores after mild sulfurization (100 mg). Next, SEM and TEM analyses of Ag/Ag_2S@ZnS-II are carried out. It is apparent from Figure 5d,e that the shell structure is still well-retained while the cubic core is partially etched which leads to subsequent Ag dissolution. Notably, in this case, higher concentration of thiourea has led to higher extent of sulfurization, hence causing the structures to be more porous, evidently from the BET analysis and morphological comparison of Figure 5b,e. Further increase in sulfurization (dosage of 300 mg thiourea) leads to the transformation/collapse of nanosheet shell into nanoparticles which yield Ag/Ag_2S@ZnS-III sample (Figure 5g,h). In order to verify a complete conversion from Zn-silicate to ZnS, EDX spectra (Figure 5c,f,i) are obtained from all three samples Ag/Ag_2S@ZnS- I, -II. and -III, respectively. It can be seen that, except for the extraneous elements, the presence of Zn, S, and Ag peaks can be observed for all samples, which is consistent with their corresponding TEM findings.

In addition, uniform and well-defined ZnS nanosheets with an absence of core as reference samples are also prepared without employing Ag nanocubes, as shown in SEM and TEM images of Figure 6a,b, respectively. The inset of Figure 6b is an HR-TEM image taken from the nanosheets. The lattice spacing is determined to be mainly 0.312 nm, corresponding to the (111) plane of zinc-blende ZnS.[35] The crystal phases of the samples are examined by XRD as shown in Figure 6c. All the indexed diffraction peaks for ZnS sample can be assigned to zinc-blende ZnS, which is consistent with previous reports.[35,36] On the other hand, zinc-blende ZnS, metallic Ag (marked with hashtags, JCPDS 65-2871), and Ag_2S (marked with stars, monoclinic: JCPDS 14-0072)[37] can be detected for sample Ag/Ag_2S@ZnS- I and -II. In comparison, the latter sample II shows lower Ag peaks intensities but of a higher Ag_2S peaks than sample I. On the other hand, no Ag diffraction peaks are

DOI: 10.1021/jp510413b
J. Phys. Chem. C 2015, 119, 1667−1675

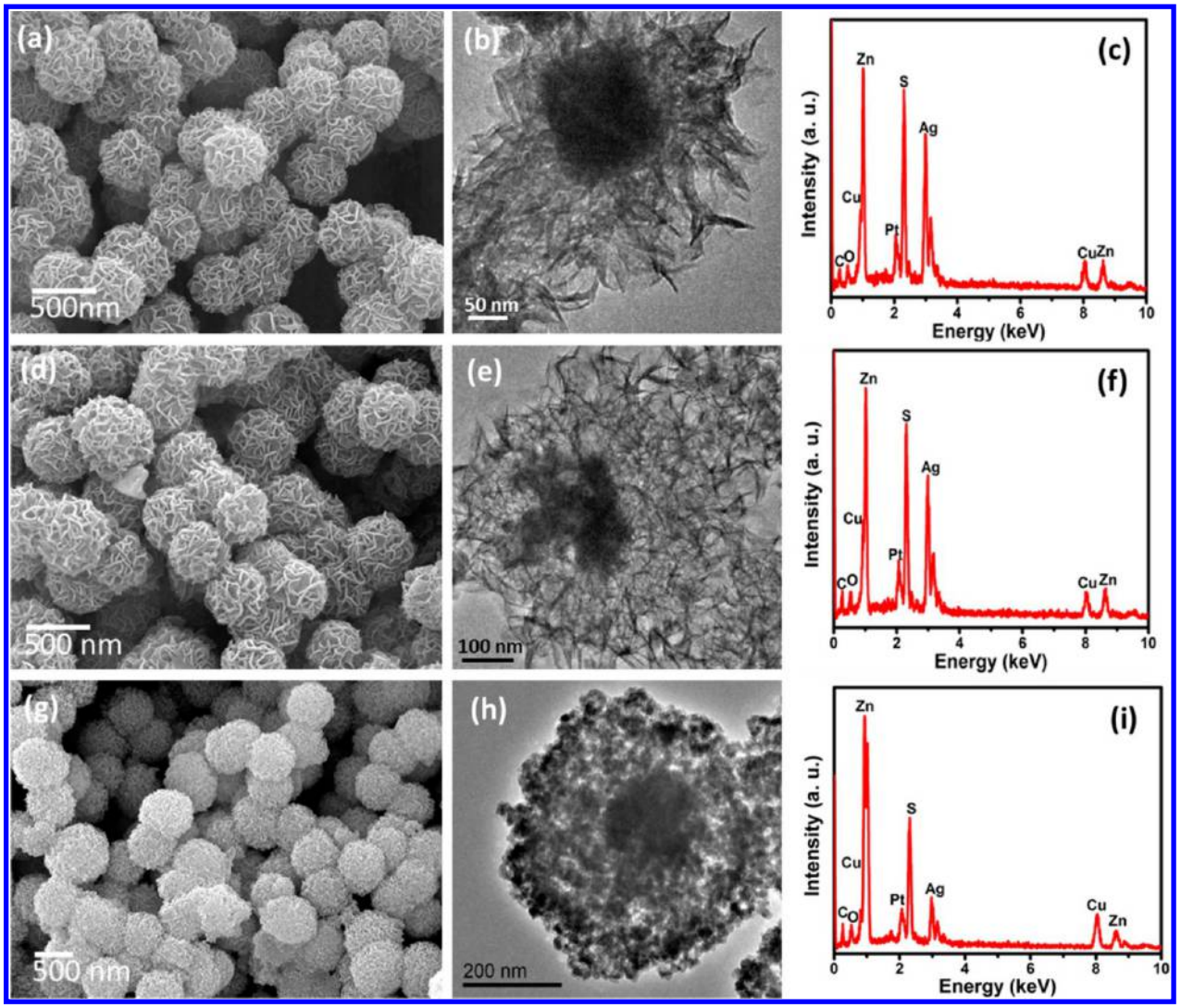

Figure 5. FESEM images (a, d, and g), TEM images (b, e, and h), and EDX patterns (c, f, and i) of the Ag/Ag_2S@ZnS-I (a–c), Ag/Ag_2S@ZnS-II (d–f), and Ag/Ag_2S@ZnS-III (g–i), respectively.

observed for Ag/Ag_2S@ZnS-III sample since Ag core has undergone complete sulfurization. This implies that, with the control of sulfurization process, the extent of Ag core dissolution–diffusion and hence chemical hybridization can possibly be manipulated.

TEM EDX mappings are performed to further study the elemental composition and elemental distribution of the core–shell structures. Figure 7a–c shows the acquired bright field TEM images for sample Ag/Ag_2S@ZnS- I, -II, and -III, respectively, where their cores transformed from fairly well-preserved cubic shaped core to partially and markedly etched cores. The Zn–K mappings (Figure 7d–f) show uniform distribution throughout the core–shell structure. The Ag-L signals of Ag/Ag_2S@ZnS- I and -II (Figure 7g,h) are confined mainly in the center portion of the structures while Ag/Ag_2S@ZnS-III exhibits more scattered Ag-L signals (Figure 7i). These observations infer a considerable localized diffusion of Ag ions to the shell structure with increase sulfurization. The partial transformation of Ag core to Ag/Ag_2S hybrid core was previously shown by XRD analyses (Figure 6c) and later verified by XPS results (Figure 8). The distributions of S shown in Figure 7j–l confirm that, with increasing sulfurization reaction, the regions representing S on the elemental maps are enlarged and expanded outward to the shell. It should be noted that the S mapping distribution comes from both the ZnS and Ag_2S. In comparison, lower amounts of Ag were dissolved and dispersed outward to the ZnS shells to form Ag_2S in Ag/Ag_2S@ZnS-I and -II samples than the Ag/Ag_2S@ZnS-III sample, leading to their smaller area and lower densities of S elements than those of Zn. In contrast, the Ag/Ag_2S@ZnS-III sample is subjected to increased sulfurization of Ag nanocubes which drives more Ag species into the ZnS shell to form a homogeneous ZnS–Ag_2S shell, making the distribution areas of Zn and S almost the same. In addition, it can be observed from the S mapping (Figure 7j–l) that the S densities of the core areas in Ag/Ag_2S@ZnS-I and -II are much higher than that of Ag/Ag_2S@ZnS-III and also the expansion of S and Ag areas are consistent with the extent of sulfurization from Ag/Ag_2S@ZnS-I to -III samples, which have clearly indicated the outward-diffusion kinetics of Ag_2S. In general, the uniformity of the hybridization between the composition elements improves with sulfurization. The control of sulfurization is the key to manipulating the composition and homogenity of the heterostructures by means of Ag core dissolution, diffusion, and recrystallization attributed to ion exchange reaction with a nonequilibrium interdiffusion mechanism.[38,39] This in situ

DOI: 10.1021/jp510413b
J. Phys. Chem. C 2015, 119, 1667–1675

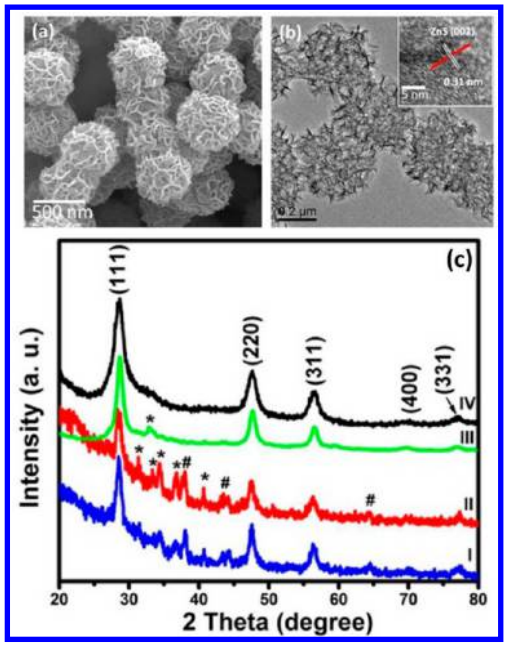

Figure 6. FESEM image (a), TEM image (b), and HRTEM (inset of b) of the ZnS nanospheres, and XRD patterns (c) of the Ag/Ag_2S@ ZnS-I, -II, -III and ZnS nanospheres (IV).

chemical transformation can facilitate intimate and homogeneous hybridization of multiphase materials within its core−shell structure.

To further investigate the chemical states of the as-prepared materials, XPS is performed (Figure 8). The binding energy of Zn $2p_{3/2}$ is allocated at 1021.5 eV, while the S 2p core-level spectra show two deconvoluted peaks with binding energies of S $2p_{3/2}$ and S $2p_{1/2}$ at 161.3 and 162.1 eV, respectively, which suggest that S is in sulfide state.[40] The control sample ZnS shows an absence of Ag while Ag $3d_{3/2}$ and Ag $3d_{5/2}$ are detected for samples Ag/Ag_2S@ZnS-I, -II, and -III. Peak fittings of Ag 3d spectra reveal that 368.2 and 374.2 eV peaks are consistent with the binding energies of Ag $3d_{5/2}$ and Ag $3d_{3/2}$ metallic Ag^0 while 367.8 and 373.8 eV peaks are ascribed to Ag $3d_{5/2}$ and Ag $3d_{3/2}$ of Ag^+ for samples Ag/Ag_2S@ZnS-I, -II. Peaks of Ag^+ are observed only for sample Ag/Ag_2S@ZnS-III, indicating the complete conversion of Ag to Ag^+. The atomic percentages of the Ag detected for the samples I and II are ∼2 and 4% while that of S are 13% and 28%, respectively. The XPS surface analysis has detected the presence of Ag 3d due to the out-diffusion of Ag species during the sulfurization process. The higher content of sulfurization may have cracked the Ag nanocubes into smaller fragments of nanosized particles. Some of these Ag nanoparticles have dispersed outward from inner core to the surface of the shell structures which can clearly be observed in Figure 7b (the small black dots embedded in the shell). Therefore, these XPS surface analyses agree with the STEM observations where substantial sulfurization and out-diffusion of Ag from the core has been extended to the shell structures which are detected by XPS.

It is noteworthy that, in addition to the presence of the Ag/Ag_2S core, the homogeneous out-diffusion and recrystallization of Ag_2S throughout the shell structure optimize contact

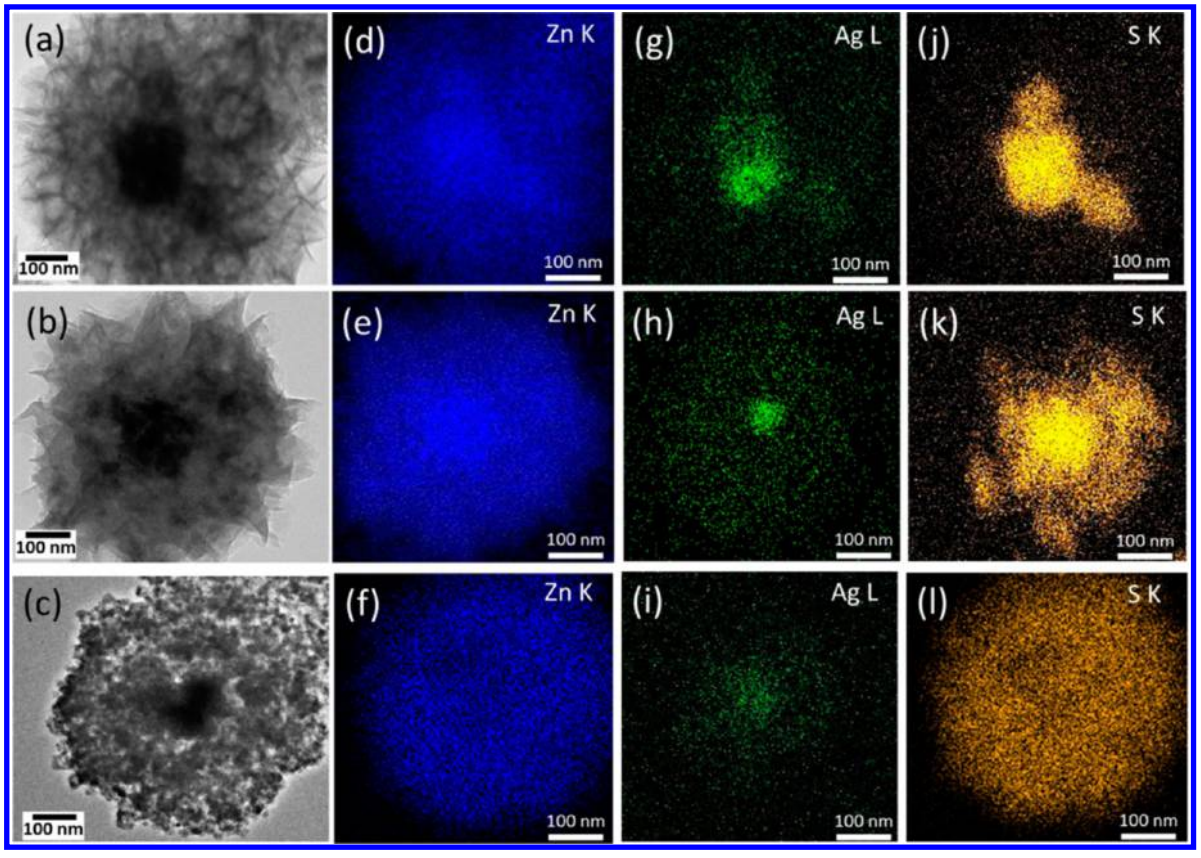

Figure 7. TEM bright field images (a−c), Zn K (d−f), Ag L (g−i), and S K (j− l) elemental mappings of samples Ag/Ag_2S@ZnS-I (a, d, g, and j), Ag/Ag_2S@ZnS-II (b, e, h, and k), and Ag/Ag_2S@ZnS-III (c, f, i, and l), respectively.

DOI: 10.1021/jp510413b
J. Phys. Chem. C 2015, 119, 1667−1675

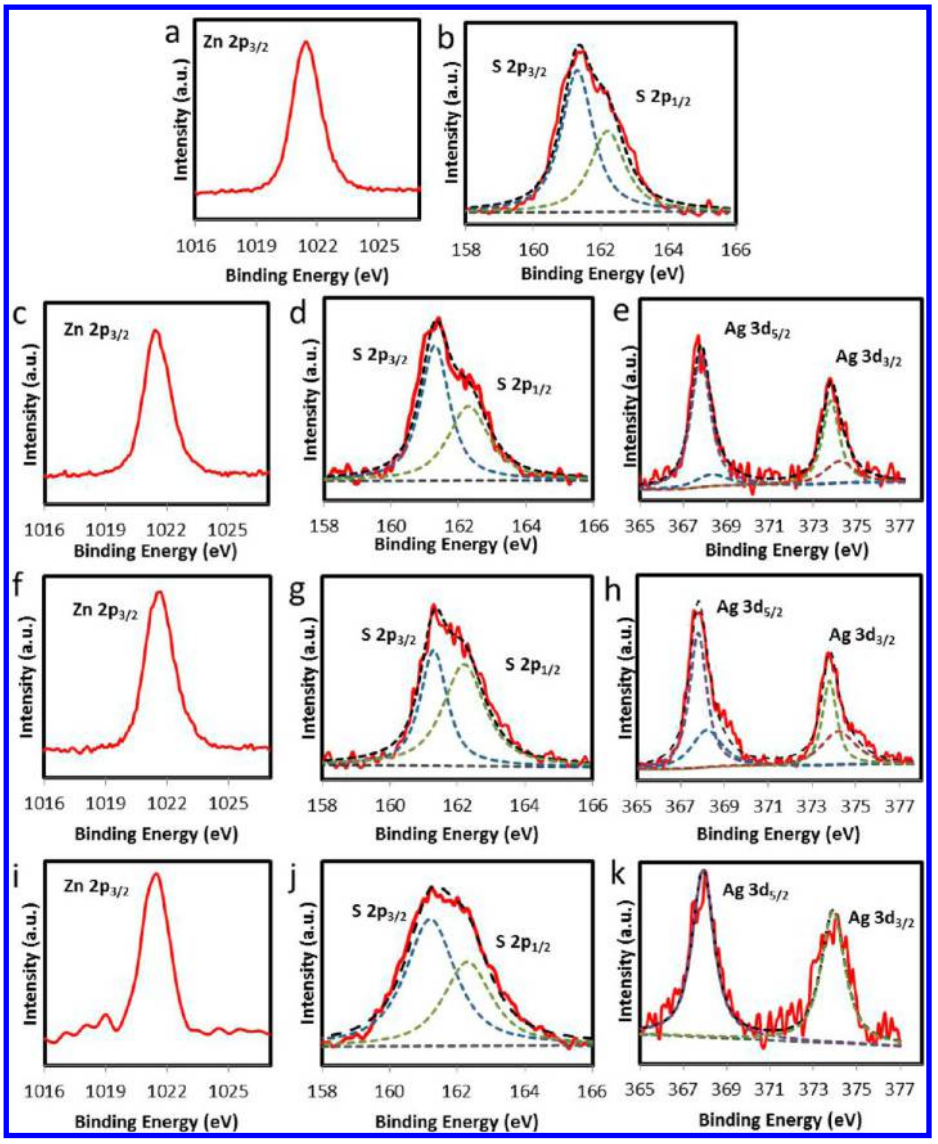

Figure 8. XPS results of sample ZnS (a and b), Ag/Ag_2S@ZnS-I (c–e), Ag/Ag_2S@ZnS-II (f–h), and Ag/Ag_2S@ZnS-III (i–k).

interface for enhanced heterojunction-induced charge transfer, an outstanding issue commonly faced in the design of a photocatalyst where cocatalyst is often surface loaded/coupled.[41−43] This rational structural fabrication and chemical hybridization approach is anticipated to be beneficial for solar-to-chemical energy conversion application. Consequently, UV–vis measurements were carried out which reveal the extended visible light absorption of sample Ag/Ag_2S@ZnS-I, -II, and -III as compared to control sample ZnS (Figure 9a). The complexity of the core–shell architecture in both structure and chemical composition may endow the materials with exceptional optical properties.[6,44−46] Previously, hybrid Ag/Ag_2S materials have been investigated for photocatalytic studies.[11,47] In this study, proof-of-concept of the multiphase hybrid Ag/Ag_2S@ZnS as UV to visible light responsive photocatalyst for enhanced solar H_2 production is demonstrated (Figure 9b). As expected, no H_2 is generated for the control samples ZnS and pure Ag and Ag_2S nanocubes, which confirms that they are not suitable for H_2 production under visible light. In contrast, multiphase Ag/Ag_2S@ZnS- I, -II, and -III heterostructures are able to show visible-light solar hydrogen production of ∼20, 25, and 46 μmol h^{-1} g^{-1}, respectively. The production rate of H_2 improves with sulfurization which can be attributed to higher content of Ag_2S (with narrow band gap of 1.1 eV and a relatively large absorption coefficient) in the shell structure which leads to enhance visible light absorption.[26,37,48−50] In addition, H_2 performances under the whole solar spectrum are evaluated (Figure 6b). The control sample (ZnS) exhibits a lower production rate (∼126 μmol h^{-1} g^{-1}) under the UV–vis range. The multiphase Ag/Ag_2S@ZnS samples produce a relatively higher amount of H_2 compared to pure ZnS, with the Ag/Ag_2S@ZnS-III being the highest production rate (∼243 μmol h^{-1} g^{-1}) sample, which is consistent with its performance under visible light. The best H_2 performance of Ag/Ag2S@ZnS-III may be due to its homogeneous hybridization of ZnS and Ag_2S, which has improved the visible-light absorption. Also, it should be noted that the out-diffusion process has hybridized the ZnS shells with smaller bandgap, Ag_2S (see Figure 7), and hence led to the formation of a new hybrid semiconductor of narrower bandgap. The hybrid material may have wider light absorbance range (see Figure 9a), and hence can promote the evolution of H_2 under visible light. It is speculated that the sulfurization process has led to the homogeneous dissolution and trans-

DOI: 10.1021/jp510413b
J. Phys. Chem. C 2015, 119, 1667−1675

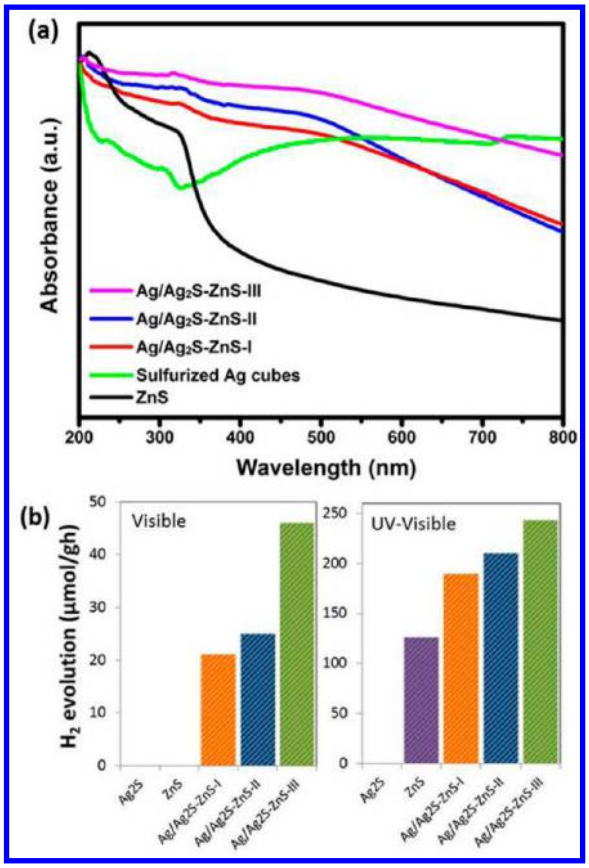

Figure 9. UV−vis absorption measurements (a) and H_2 evolution of the as-prepared samples (b) under visible and UV−vis light irradiation.

formation into hybrid solid solution composite of narrower bandgap, which enhances light absorption and increases H_2 production rates.

4. CONCLUSIONS

We have integrated distinctive structures (nanocube and nanosheets) and chemical composition materials to form multiphase Ag/Ag_2S@ZnS core−shell structures through hydrothermal synthesis and sulfurization. The chemical transformation of Zn silicate to ZnS shell and dissolution−recrystallization of Ag cores to promote homogeneous hybridization of multiphase structure can be realized by one-step sulfurization process. Finally, this work demonstrates a proof of concept on the feasibility of employing the as-prepared multiphase Ag/Ag_2S@ZnS core−shell heterostructures as visible to UV light responsive photocatalyst.

AUTHOR INFORMATION

Corresponding Author

*E-mail: elehgw@nus.edu.sg. Phone: (65) 6516 8121. Fax: (65) 6775 4710.

Notes

The authors declare no competing financial interest.

ACKNOWLEDGMENTS

The work was financially supported by MOE Grant R-263-000-653/654-731/112 and A*star R-263-000-A96-305.

REFERENCES

(1) Cozzoli, P. D.; Pellegrino, T.; Manna, L. Synthesis, Properties and Perspectives of Hybrid Nanocrystal Structures. *Chem. Soc. Rev.* **2006**, *35*, 1195−1208.

(2) Pellegrino, T.; Fiore, A.; Carlino, E.; Giannini, C.; Cozzoli, P. D.; Ciccarella, G.; Respaud, M.; Palmirotta, L.; Cingolani, R.; Manna, L. Heterodimers Based on Copt3-Au Nanocrystals with Tunable Domain Size. *J. Am. Chem. Soc.* **2006**, *128*, 6690−6698.

(3) Jiang, J.; Gu, H. W.; Shao, H. L.; Devlin, E.; Papaefthymiou, G. C.; Ying, J. Y. Manipulation Bifunctional Fe3O4-Ag Heterodimer Nanoparticles for Two-Photon Fluorescence Imaging and Magnetic Manipulation. *Adv. Mater.* **2008**, *20*, 4403−4407.

(4) Tsuji, I.; Kato, H.; Kobayashi, H.; Kudo, A. Photocatalytic H-2 Evolution Reaction from Aqueous Solutions over Band Structure-Controlled (Agin)(X)Zn2(1-X)S2 Solid Solution Photocatalysts with Visible-Light Response and Their Surface Nanostructures. *J. Am. Chem. Soc.* **2004**, *126*, 13406−13413.

(5) Pang, X. C.; Zhao, L.; Han, W.; Xin, X. K.; Lin, Z. Q. A General and Robust Strategy for the Synthesis of Nearly Monodisperse Colloidal Nanocrystals. *Nat. Nanotechnol.* **2013**, *8*, 426−431.

(6) Zhu, T.; Wu, H. B.; Wang, Y. B.; Xu, R.; Lou, X. W. Formation of 1D Hierarchical Structures Composed of Ni3s2 Nanosheets on Cnts Backbone for Supercapacitors and Photocatalytic H2 Production. *Adv. Energy Mater.* **2012**, *2*, 1497−1502.

(7) Zhao, Q.; Ji, M.; Qian, H.; Dai, B.; Weng, L.; Gui, J.; Zhang, J.; Ouyang, M.; Zhu, H. Controlling Structural Symmetry of a Hybrid Nanostructure and Its Effect on Efficient Photocatalytic Hydrogen Evolution. *Adv. Mater.* **2014**, *26*, 1387−1392.

(8) Chaudhuri, R. G.; Paria, S. Core/Shell Nanoparticles: Classes, Properties, Synthesis Mechanisms, Characterization, and Applications. *Chem. Rev.* **2012**, *112*, 2373−2433.

(9) Wang, Y. R.; Yang, W. L.; Zhang, L.; Hu, Y.; Lou, X. W. Formation of Ms-Ag and Ms (M = Pb, Cd, Zn) Nanotubes Via Microwave-Assisted Cation Exchange and Their Enhanced Photocatalytic Activities. *Nanoscale* **2013**, *5*, 10864−10867.

(10) Awazu, K.; Fujimaki, M.; Rockstuhl, C.; Tominaga, J.; Murakami, H.; Ohki, Y.; Yoshida, N.; Watanabe, T. A Plasmonic Photocatalyst Consisting of Sliver Nanoparticles Embedded in Titanium Dioxide. *J. Am. Chem. Soc.* **2008**, *130*, 1676−1680.

(11) Yang, W. L.; Zhang, L.; Hu, Y.; Zhong, Y. J.; Wu, H. B.; Lou, X. W. Microwave-Assisted Synthesis of Porous Ag2s-Ag Hybrid Nanotubes with High Visible-Light Photocatalytic Activity. *Angew. Chem., Int. Ed.* **2012**, *51*, 11501−11504.

(12) Yu, J. G.; Qi, L. F.; Jaroniec, M. Hydrogen Production by Photocatalytic Water Splitting over Pt/Tio2 Nanosheets with Exposed (001) Facets. *J. Phys. Chem. C* **2010**, *114*, 13118−13125.

(13) Yang, M.-Q.; Zhang, N.; Pagliaro, M.; Xu, Y.-J. Artificial Photosynthesis over Graphene-Semiconductor Composites. Are We Getting Better? *Chem. Soc. Rev.* **2014**, *43*, 8240−8254.

(14) Zhang, N.; Zhang, Y. H.; Xu, Y. J. Recent Progress on Graphene-Based Photocatalysts: Current Status and Future Perspectives. *Nanoscale* **2012**, *4*, 5792−5813.

(15) Yang, M. Q.; Xu, Y. J. Selective Photoredox Using Graphene-Based Composite Photocatalysts. *Phys. Chem. Chem. Phys.* **2013**, *15*, 19102−19118.

(16) Li, W.; Deng, Y. H.; Wu, Z. X.; Qian, X. F.; Yang, J. P.; Wang, Y.; Gu, D.; Zhang, F.; Tu, B.; Zhao, D. Y. Hydrothermal Etching Assisted Crystallization: A Facile Route to Functional Yolk-Shell Titanate Microspheres with Ultrathin Nanosheets-Assembled Double Shells. *J. Am. Chem. Soc.* **2011**, *133*, 15830−15833.

(17) Chen, Y.; Chen, H. R.; Guo, L. M.; He, Q. J.; Chen, F.; Zhou, J.; Feng, J. W.; Shi, J. L. Hollow/Rattle-Type Mesoporous Nanostructures by a Structural Difference-Based Selective Etching Strategy. *ACS Nano* **2010**, *4*, 529−539.

(18) Huang, X. Q.; Guo, C. Y.; Zuo, L. Q.; Zheng, N. F.; Stucky, G. D. An Assembly Route to Inorganic Catalytic Nanoreactors Containing Sub-10-Nm Gold Nanoparticles with Anti-Aggregation Properties. *Small* **2009**, *5*, 361−365.

DOI: 10.1021/jp510413b
J. Phys. Chem. C 2015, 119, 1667−1675

(19) Zhang, N.; Liu, S. Q.; Xu, Y. J. Recent Progress on Metal Core@ Semiconductor Shell Nanocomposites as a Promising Type of Photocatalyst. *Nanoscale* **2012**, *4*, 2227−2238.
(20) Zhang, N.; Xu, Y. J. Aggregation- and Leaching-Resistant, Reusable, and Multifunctional Pd@Ceo2 as a Robust Nanocatalyst Achieved by a Hollow Core-Shell Strategy. *Chem. Mater.* **2013**, *25*, 1979−1988.
(21) Zhang, N.; Fu, X. Z.; Xu, Y. J. A Facile and Green Approach to Synthesize Pt@Ceo2 Nanocomposite with Tunable Core-Shell and Yolk-Shell Structure and Its Application as a Visible Light Photocatalyst. *J. Mater. Chem.* **2011**, *21*, 8152−8158.
(22) Liu, S.; Zhang, N.; Xu, Y.-J. Core−Shell Structured Nanocomposites for Photocatalytic Selective Organic Transformations. *Part. Part. Syst. Charact.* **2014**, *31*, 540−556.
(23) Qiu, X. Q.; et al. Hybrid CuxO/TiO2 Nanocomposites as Risk-Reduction Materials in Indoor Environments. *ACS Nano* **2012**, *6*, 1609−1618.
(24) Zhang, N.; Liu, S. Q.; Fu, X. Z.; Xu, Y. J. Synthesis of M@TiO2 (M = Au, Pd, Pt) Core-Shell Nanoconnposites with Tunable Photoreactivity. *J. Phys. Chem. C* **2011**, *115*, 9136−9145.
(25) Jiang, W. Q.; Zhou, Y. F.; Zhang, Y. L.; Xuan, S. H.; Gong, X. L. Superparamagnetic Ag@Fe3O4 Core-Shell Nanospheres: Fabrication, Characterization and Application as Reusable Nanocatalysts. *Dalton Trans.* **2012**, *41*, 4594−4601.
(26) Chaudhuri, R. G.; Paria, S. Optical Properties of Double-Shell Hollow ZnS-Ag2S Nanoparticles. *J. Phys. Chem. C* **2013**, *117*, 23385−23390.
(27) Guo, W. C.; Wang, Q.; Wang, G.; Yang, M.; Dong, W. J.; Yu, J. Facile Hydrogen-Bond-Assisted Polymerization and Immobilization Method to Synthesize Hierarchical Fe3O4@Poly(4-Vinylpyridine-Co-Divinylbenzene)@Au Nanostructures and Their Catalytic Applications. *Chem.—Asian J.* **2013**, *8*, 1160−1167.
(28) Geng, J. L.; Liu, J.; Liang, J.; Shi, H. B.; Liu, B. A General Approach to Prepare Conjugated Polymer Dot Embedded Silica Nanoparticles with a SiO2@Cp@SiO2 Structure for Targeted Her2-Positive Cellular Imaging. *Nanoscale* **2013**, *5*, 8593−8601.
(29) Tsuji, M.; Ikedo, K.; Uto, K.; Matsunaga, M.; Yoshida, Y.; Takemura, K.; Niidome, Y. Formation of Au@Pd@Cu Core-Shell Nanorods from Au@Pd Nanorods through a New Stepwise Growth Mode. *CrystEngComm* **2013**, *15*, 6553−6563.
(30) Tsuji, M.; Matsunaga, M.; Kumagai, H.; Ogino, M.; Hikino, S.; Yoshida, Y.; Ishizaki, T. Synthesis of Au@Ag@Cu Trimetallic Nanocrystals Using Three-Step Reduction. *CrystEngComm* **2013**, *15*, 1345−1351.
(31) Pang, X. C.; Wan, C. S.; Wang, M. Y.; Lin, Z. Q. Strictly Biphasic Soft and Hard Janus Structures: Synthesis, Properties, and Applications. *Angew. Chem., Int. Ed.* **2014**, *53*, 5524−5538.
(32) Ye, M. D.; Wang, M. Y.; Zheng, D. J.; Zhang, N.; Lin, C. J.; Lin, Z. Q. Garden-Like Perovskite Superstructures with Enhanced Photocatalytic Activity. *Nanoscale* **2014**, *6*, 3576−3584.
(33) Yang, J. P.; Shen, D. K.; Zhou, L.; Li, W.; Li, X. M.; Yao, C.; Wang, R.; El-Toni, A. M.; Zhang, F.; Zhao, D. Y. Spatially Confined Fabrication of Core-Shell Gold Nanocages@Mesoporous Silica for near-Infrared Controlled Photothermal Drug Release. *Chem. Mater.* **2013**, *25*, 3030−3037.
(34) Zhu, M. S.; Chen, P. L.; Liu, M. H. Sunlight-Driven Plasmonic Photocatalysts Based on Ag/Agcl Nanostructures Synthesized Via an Oil-in-Water Medium: Enhanced Catalytic Performance by Morphology Selection. *J. Mater. Chem.* **2011**, *21*, 16413−16419.
(35) Li, S. K.; Wu, Z. G.; Li, W. H.; Liu, Y.; Zhuo, R. F.; Yan, D.; Jun, W.; Yan, P. X. One-Pot Synthesis of Zns Hollow Spheres Via a Low-Temperature, Template-Free Hydrothermal Route. *CrystEngComm* **2013**, *15*, 1571−1577.
(36) Dawood, F.; Schaak, R. E. ZnO-Templated Synthesis of Wurtzite-Type Zns and Znse Nanoparticles. *J. Am. Chem. Soc.* **2009**, *131*, 424−425.
(37) Shen, S. L.; Zhang, Y. J.; Peng, L.; Du, Y. P.; Wang, Q. B. Matchstick-Shaped Ag2S-ZnS Heteronanostructures Preserving Both Uv/Blue and near-Infrared Photoluminescence. *Angew. Chem., Int. Ed.* **2011**, *50*, 7115−7118.
(38) Wang, D. S.; Xie, T.; Peng, Q.; Li, Y. D. Ag, Ag2S, and Ag2Se Nanocrystals: Synthesis, Assembly, and Construction of Mesoporous Structures. *J. Am. Chem. Soc.* **2008**, *130*, 4016−4022.
(39) Fan, W. G.; Jewell, S.; She, Y. Y.; Leung, M. K. H. In Situ Deposition of Ag-Ag2s Hybrid Nanoparticles onto Tio2 Nanotube Arrays Towards Fabrication of Photoelectrodes with High Visible Light Photoelectrochemical Properties. *Phys. Chem. Chem. Phys.* **2014**, *16*, 676−680.
(40) Pang, M. L.; Zeng, H. C. Highly Ordered Self-Assemblies of Submicrometer Cu2O Spheres and Their Hollow Chalcogenide Derivatives. *Langmuir* **2010**, *26*, 5963−5970.
(41) Kudo, A.; Miseki, Y. Heterogeneous Photocatalyst Materials for Water Splitting. *Chem. Soc. Rev.* **2009**, *38*, 253−278.
(42) Yerga, R. M. N.; Galvan, M. C. A.; del Valle, F.; de la Mano, J. A. V.; Fierro, J. L. G. Water Splitting on Semiconductor Catalysts under Visible-Light Irradiation. *ChemSusChem* **2009**, *2*, 471−485.
(43) Shimura, K.; Yoshida, H. Heterogeneous Photocatalytic Hydrogen Production from Water and Biomass Derivatives. *Energy Environ. Sci.* **2011**, *4*, 2467−2481.
(44) Zhang, L.; Wu, H. B.; Lou, X. W. Metal-Organic-Frameworks-Derived General Formation of Hollow Structures with High Complexity. *J. Am. Chem. Soc.* **2013**, *135*, 10664−10672.
(45) Shuai, X. M.; Shen, W. Z. A Facile Chemical Conversion Synthesis of Zno/Zns Core/Shell Nanorods and Diverse Metal Sulfide Nanotubes. *J. Phys. Chem. C* **2011**, *115*, 6415−6422.
(46) Zhang, F.; Braun, G. B.; Shi, Y. F.; Zhang, Y. C.; Sun, X. H.; Reich, N. O.; Zhao, D. Y.; Stucky, G. Fabrication of Ag@Sio2@Y2o3:Er Nanostructures for Bioimaging: Tuning of the Upconversion Fluorescence with Silver Nanoparticles. *J. Am. Chem. Soc.* **2010**, *132*, 2850−2851.
(47) Jiang, F. R.; Tian, Q. W.; Tang, M. H.; Chen, Z. G.; Yang, J. M.; Hu, J. Q. One-Pot Synthesis of Large-Scaled Janus Ag-Ag2S Nanoparticles and Their Photocatalytic Properties. *CrystEngComm* **2011**, *13*, 7189−7193.
(48) Zhang, H. L.; Wei, B.; Zhu, L.; Yu, J. H.; Sun, W. J.; Xu, L. L. Cation Exchange Synthesis of Zns-Ag2s Microspheric Composites with Enhanced Photocatalytic Activity. *Appl. Surf. Sci.* **2013**, *270*, 133−138.
(49) Zhang, J.; Liu, S. W.; Yu, J. G.; Jaroniec, M. A Simple Cation Exchange Approach to Bi-Doped Zns Hollow Spheres with Enhanced UV and Visible-Light Photocatalytic H-2-Production Activity. *J. Mater. Chem.* **2011**, *21*, 14655−14662.
(50) Li, Q.; Meng, H.; Zhou, P.; Zheng, Y. Q.; Wang, J.; Yu, J. G.; Gong, J. R. Zn1-Xcdxs Solid Solutions with Controlled Bandgap and Enhanced Visible-Light Photocatalytic H-2-Production Activity. *ACS Catal.* **2013**, *3*, 882−889.

DOI: 10.1021/jp510413b
J. Phys. Chem. C 2015, 119, 1667−1675